Journal of Applied Fluid Mechanics, Vol. 9, No. 2, pp. 1023-1034, 2016.
Available online at www.jafmonline.net, ISSN 1735-3572, EISSN 1735-3645.
DOI: 10.18869/acadpub.jafm.68.225.24442

A 3-D Moving Mesh Method for Simulation of Flow around a Rotational Body

M. M. Razzaghi[1†] and S. M. Mirsajedi[2]

[1]*Department of aerospace engineering, Science and Research branch, Islamic Azad University, Tehran, Iran*
[2]*Faculty of new technologies engineering, Shahid Beheshti University, Tehran, Iran*

†*Corresponding Author Email:razzaghi@pmc.iaun.ac.ir*

(Received December 31, 2014; accepted June 24, 2015)

ABSTRACT

The numerical simulation of flow around a three dimensional moving body faces different problems in several methods, such as disruption of the structure of the grid, the need for deletion and insertion of nodes, interpolation, and data transfer between different parts of grid. In order to tackle the above-mentioned problems, a new configuration has been developed for meshing domain, which besides providing the body with the capability of rotational and oscillatory motions in large displacements, saves the grid's primitive quality. In the introduced method, the grid connections are manipulated with the motion of the body, but the general form of the grid is not changed or disrupted. This needs a special form for nodes of the grid, which is explained in this paper. The three dimensional unsteady form of the Euler equations is solved and the properties over each cell faces are evaluated using an averaging method. For time integration of the equations an implicit dual time method is used. It can prove that the volume of all elements is constant in the introduced grid. Therefore, there is no need to calculate elements volume in every time step. Several test cases are solved and the results are compared with experimental or other numerical data.

Keywords: Three dimensional; Moving body; Oscillation; Grid connection; Unsteady.

NOMENCLATURE

C_p	pressure coefficient
C_n	normal force coefficient
C_m	pitching moment coefficient
c	chord
E	total energy
F	convective flux in the x direction
G	convective flux in the y direction
H	convective flux in the z direction
K	reduce frequency
M	Mach number
P	pressure
Q	vector of conserved variable
S	surface
t	time
ux	component of Cartesian velocity
vy	component of Cartesian velocity
w	z component of Cartesian velocity
u_r	relative velocity in the x direction
v_r	relative velocity in the y direction
w_r	relative velocity in the z direction
V	volume
x_t	velocity of control-volume boundary in the x direction
y_t	velocity of control-volume boundary in the y direction
z_t	velocity of control-volume boundary in the z direction
α	angle of attack
γ	ratio of specific heat
ρ	density
τ	pseudo-time
ω	angular frequency

1. INTRODUCTION

Simulation of flow around a 3-D moving body can, in view of its various applications in sciences and engineering, prove very useful. Particularly in aerospace science, modeling the rotational motions of aerospace vehicles around various axes, maneuvers of aircrafts and movement of blades of articulated rotors in helicopters which have 3-D rotation, the three dimensional simulation is needed.

Numerical simulation of flow consists of two general steps, the first step involves computational

grid generation in solution domain and the second step involves analysis of flow with using the selected method. The primitive grid becomes useless as body is displaced; therefore, the numerical simulation of flow around a moving body needs an efficient computational grid; an intelligent grid able to intelligently adapt itself to the motion of body. This is especially needed in three dimensional spaces and large motions.

The first method in this regard is regeneration of the grid after each body motion and modification of boundaries which are not acceptable because of repeated interpolations and time consumption (Goswami and Parpia 1991; Gaitonde and Fiddes 1995).

In the dynamic grid, the motions of the body are transferred to grid elements. Batina (1989) assumed that the nodes in the domain are inter-connected via springs. After each change in body location, a smoothening process is performed through the balancing of the spring force. Spring factor is selected by the user, and the first choice is selection of the same spring factor for all of springs (Hase, Anderson, and Parpia 1991). The other choice is selection of the spring factor with the reverse of the distance between two nodes, which causes the nodes that are closer to have smaller displacements and, hence, the reduction of grid quality is delayed. In complex geometries and large motions of the body, to prevent the interference of elements, the angle between nodes connection is taken into consideration in, the definition of the spring elasticity coefficient (Batina, 1991; Pirzadeh, 1999). Use of torsion springs near linear springs is another strategy that has been considered (Degand and Farhat 2002; Zeng and Ethier 2005). Generally, using this technique in large motions can reduce grid quality and, in some cases, grid regeneration is needed locally.

In order to tackle the aforementioned problems and keep the quality of elements surrounding the body, in the moving zonal grid, the motions are transferred to elements of a layer that is selected around and far from the body. The elements of this layer are larger and their quality is reduced later (Zhang and Wang 2004). The method of choosing this layer is different in various methods and is time-consuming, with decreasing elements quality of this layer a new layer must be considered. For solving this problem**,** Mirsajedi, Karimian, and Mani (2006) and Mirsajedi and Karimian (2006a, 2006b) used a circular layer of elements in two dimensions and cylindrical shell in three dimensions. Therefore a body can rotate without any limitation in two dimensions but in three dimensions is limited around one of the three axes e.g. rolling, pitching or yawing.

Overset grid is composed of two grids: the main grid and the local grid. The local grid, along with the body, moves on the main grid. Data transfer between the two grids is very difficult and usually needs a structured grid or the unstructured Cartesian grid. Recently, unstructured grids are also used in the overset grid method. Since several interpolations are required in this method, special attention should be given to the accuracy of the method (Togashi, Ito, Nakahashi, and Obayashi, 2006; Liu and Akay, 2010; Kannan and Wang 2007; Kannan and Wang 2006; Cai, Tsai and Liu 2005).

Additional details and some of the applications of the mentioned methods are presented in references: Karimian and Ardakani (2011); Younis, Bibi, Haque and Khushnood (2009); Srinivasa Rao and Babu (2013); Ou and Jameson (2010); Ou, Castonguay and Jameson (2011); Ou and Jameson (2011) and Kamkar, Wissink, Sankaran and Jameson (2012).

Most of the current methods attempt to fix grid connections as much as possible, which leads to reduction of the amount of grid quality and limitation body motions. For solving above mentioned problems and developing method of Mirsajedi and Karimian (2006a), introduces a new algorithm for simulation of flow around a body with rotational motion. In this algorithm, making regular and foreseeable changes in grid connection, besides modeling the large motions of the body, the original grid quality is preserved, and there is no need for local regeneration or deletion/insertion of nodes, interpolation of properties, and transfer of data between to the regions.

In order to model the simultaneous rotation in different directions, three nesting sphere regions around the body were considered, each of which covered the rotation around one axis i.e. pitch, roll and yaw, and therefore, the rotational motion of the body was obtained in general. Elements of each region rotate rigidly and only one spherical shell between two the regions is deformed. To keep the quality of the grid in the rotational motion of the body, the grid adapts itself to the new rotation by manipulating the connections.

Therefore, in order to have a regular scheme for connection manipulations, the surface elements on each sphere must have rotational symmetry around an axis. This is obtained by using a circuit and meridian form for dividing the surface of each sphere. This form has a rotational symmetry around the axis that crosses two sphere poles.

The unsteady form of the Euler equations is solved and the properties over each cell faces are evaluated using an averaging method, in this method added numerical dissipative term to equations with using Jameson method (Jameson, Schmidt, and Turkel 1981; Jameson and Mavriplis 1986). For time integration of equations used an implicit dual time method (Jameson 1991; Gaitonde 1994; Jahangirian and Hadidoolabi 2004). Considering the fixedness of the volume of elements in rotational motions of the body in the introduced grid, there is no need to calculate elements volume in every time step therefore the calculations decreases. However, to accelerate convergence, local pseudo-time stepping, enthalpy damping and residual averaging are used (Jameson, Schmidt, and Turkel 1981). For more evaluation of this method during body rotation, several test cases are solved and discussed in this paper.

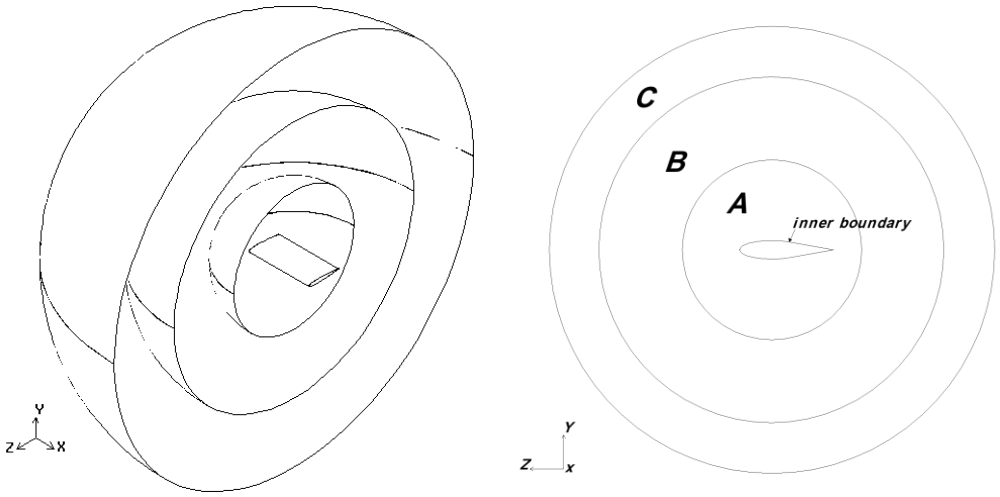

a) 3-D view **b) 2D view**

Fig. 1. Three spheres cut around the 3-D body (airplane wing).

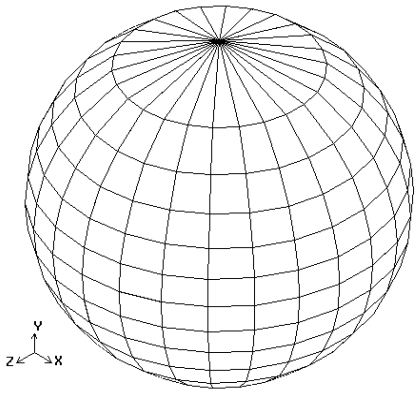

Fig. 2. Circuit and meridian form.

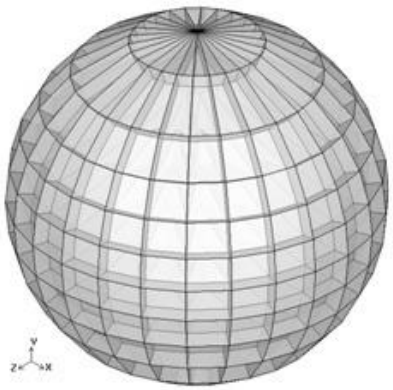

Fig. 3. Form of elements in spherical shell.

2. GRID CONFIGURATION

Every rotational motion of the body can be divided into rotation around x-axis, y-axis and z-axis. For each rotation mentioned, one spherical region is considered around body. Region (A) starts at the body surface and continues to the surface of the interior sphere; region (B) covers the space between the interior sphere and the middle sphere; and finally, region (C) begins from the middle sphere and continues to the outer sphere. The three regions are cut around a wing, as illustrated in Fig. 1.

If we assume the interior sphere for rotation around x-axis, the middle sphere for rotation around y-axis, and the outer sphere for rotation around z-axis, when the body rotates around axis-x, the interior sphere must rotate around x-axis along with the elements of Region (A); and when the body rotates around axis-y, the middle sphere along with the elements of Region (A) and (B) will rotate around the y-axis. Accordingly, for the body to rotate around the z-axis, the outer sphere along with the elements of Regions (A), (B) and (C) must rotate around the z-axis. Therefore, the rotation of the body in any direction and at the same time is possible.

But this method is not complete yet, because with the rotation of spheres, boundary elements between each neighboring pairs of regions are deformed and their quality is extremely reduced. To solve this problem, in the boundary of each pair of regions, a spherical shell is used in which the deformation is transferred to these elements. This has two advantages: first the deformed elements are completely clear and there is no need to search all of domain to find them; and, second, the deformable elements are far from the body surface.

Considering the intended idea based on the manipulation of the grid connections with the rotation of the body, surface elements must have symmetric rotation. If it was possible to achieve a form of the surface elements that have symmetric rotation in every direction, the use of three spheres would not be necessary and a single sphere would be enough, Of course this is impossible. Therefore the surface of each sphere must be divided into the circuit and meridian form. As illustrated in Fig. 2, except the elements located at the two poles of the sphere, other elements have a square surface, and the elements near the poles have triangular form.

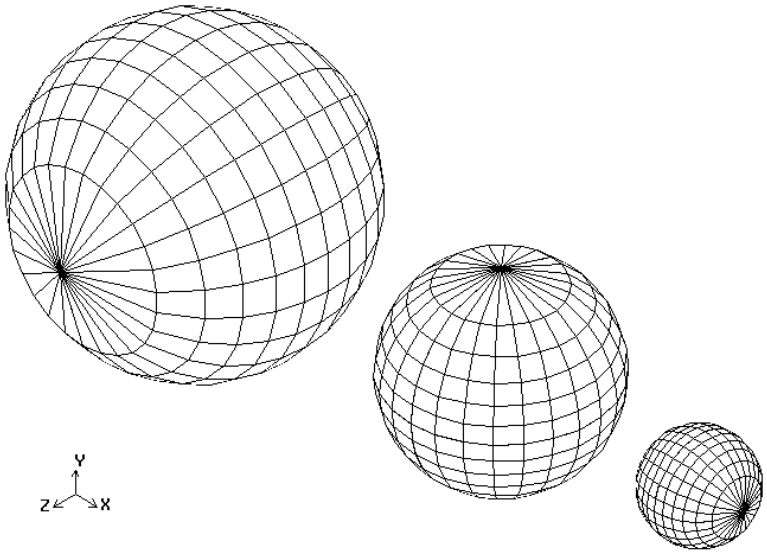

Fig. 4. Three spheres with different radii.

It should be noted that the inner and outer surfaces of each shell must have the same meshing so that the majority of the elements of the deformable shell have a hexahedral and cubic form and other elements that are near the two poles have a wedge-like form (Fig. 3).

Considering the fact that rotation in the other two perpendicular directions is needed to achieve the general modeling of the body, the surface of the other spheres must be divided in the same way; i.e., the surface of the shell in each sphere must be meshed with circuit and meridian forms, with the difference being that the axis passing through the two poles is along one of the coordinate axes in each of the spheres. This causes each sphere to have symmetric rotation around one coordinate axis and that is used as rotation around that axis. As mentioned earlier, in order to have the three rotational motions in one body, the radii of the spheres must be different (Fig. 4).

3. ESTIMATION OF THE DOMAIN DIMENSIONS

In this section, the factors effective on determining the dimension of the domain are investigated. The radius of the internal sphere should be in such a way that it totally covers the moving body and the required space for arranging qualified elements, from the surface of the moving body to the surface of the sphere (region A) existed.

The middle sphere which covers the internal sphere should have a larger radius than that of the internal one and regarding the difference between the mode of positioning surface elements of the two internal and middle spheres, the amount of increasing the radius is so much that the elements of the region (B) have the capability of matching itself from the surface mesh of the internal sphere to the surface mesh of the middle sphere. In case of insufficiency of this distance, elements will not enjoy required quality.

Furthermore, the external sphere which covers the two internal and middle spheres naturally should have a larger radius than those of the two previous ones and like the middle, with considering the surface elements of the middle and external sphere which are located in two opposite direction, the value of the radius is determined in such a way that the elements of the region (C) be qualified.

Considering this point is important that the defined regions, as much as possible, should have smaller dimensions because in this case, producing elements and consequently required controls on them decreases and the capability of simulating some moving body simultaneously increase in the solution domain.

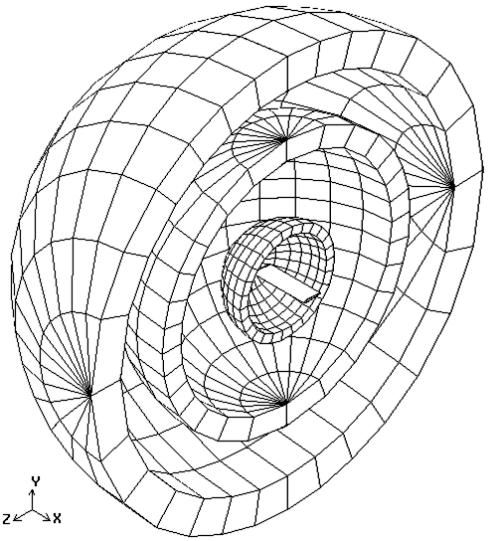

Fig. 5. Three spherical shell cut around the 3-D body (airplane wing).

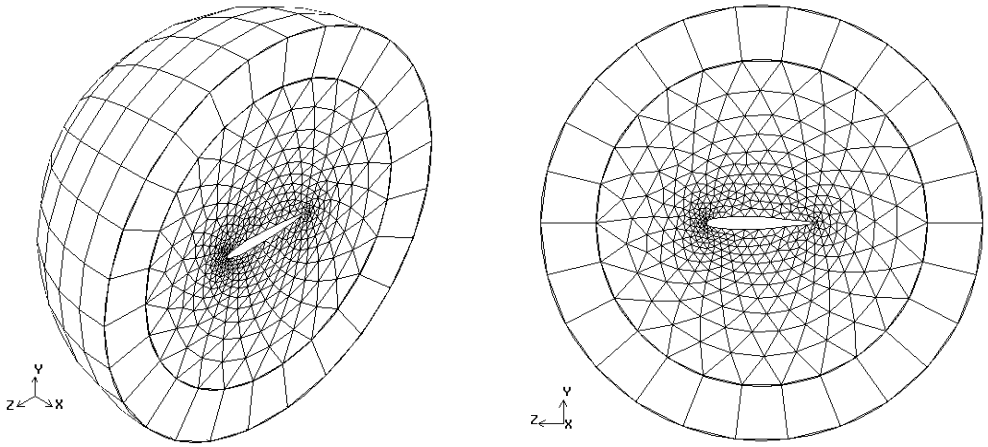

a) 3-D view **b) 2D view**

Fig. 6. Interior sphere and shell around a wing cut along the equator.

The thickness of the deformable shell composed of one element should be determined regarding the dimensions of the surface elements of the sphere, in fact we pursue the cubic elements of the shell to get more symmetric in order that the applied deformations in the distance between two stages of the manipulations in grid connections decrease less the quality of the elements of this shell; therefore, the smaller the surface elements of the sphere are, the thickness of the deformable shell are less considered and vice versa, by increasing the surface elements of the sphere, the thickness of the deformable shell increases. By considering this factor, the thickness of the deformable shell is considered as equal to the mean of two dimensions of the surface elements of the spheres.

The number of the circuits are considered in such a way that the surface elements of spheres be shaped in the form of isosceles triangles and squares as much as possible. With this in mind, the number of the circuits depends on the number of the meridians and by increasing the number of the meridians, the number of circuits increases.

The number of the meridians is available for users, but it should at least be so many that the grid can cover the curvature of the sphere and consequently by increasing the number of the meridians, more compliance will be established between the grid surface and the sphere surface. However, it should be consider that the increase in the number of the meridians and consequently the circuits and surface and volume elements will engender specific problems. (Fig. 5)

4. GRID OPERATION

To figure out the operation of the grid, the inner-most sphere along with shell is selected and the changes made in it after body motions and its special manner of adapting to the changes is described. Naturally, the two other spheres have similar manner.

A rectangular wing with NACA0012 airfoil is used for moving body. If we assume that the surface elements of the interior sphere are such that the main axis of the sphere that passes through its two poles is perpendicular to the surface of the paper, by cutting it along the equator (middle circuit) can we observe the internal part as shown in Fig. 6. It is obvious in this figure that by dividing the body surface with unstructured element, the region between body and spherical shell is filled with tetrahedral elements and only a few pyramidal elements in this region are adjacent to the spherical shell and exist in the sections that have the square surface elements. As it was previously pointed out, shell elements have a cubic form and just near the two poles have a wedge-like form.

After the rotation or oscillation of the body, all nodes and elements in the sphere move rigidly along with the body and are not deformed.

This way, the quality of the grid near the body is maintained. Only the nodes on the outer part of the shell remain fixed and do not move; therefore, the elements in the shell are deformed. Fig. 7 illustrates the grid after rotation.

With increase in rotation, the quality of the shell elements is reduced and the elements are deformed badly. In order to remedy this drawback, by manipulating the connections of the elements in this region, the component nodes of each element change. Considering the fact that angular distance of nodes in circuits of sphere are equal, in this process when each node on the inner part of the shell reaches the previous position of its neighbor node, a new connection between two nodes vis-à-vis comes to existence (Fig. 8). As it is evident, no node is deleted or inserted, but as the connections are manipulated, the structure of elements in the shell is modified and the grid returns to its original quality. Figure 9 displays the motion of the inner nodes in one circuit of the shell as well as manipulation of connections for one phase. Moreover, changes in data structure of the shell in one circuit are shown in Table 1.

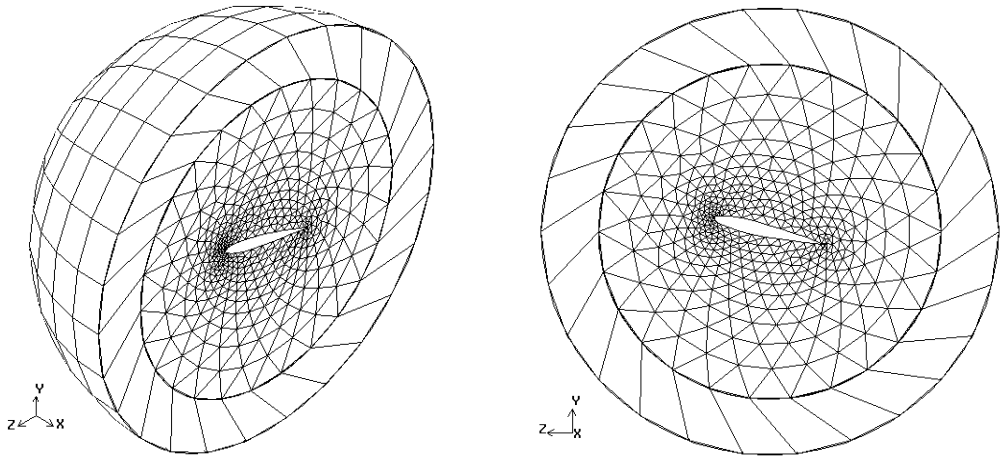

a) 3-D view **b) 2D view**

Fig. 7. Interior sphere and shell after wing rotation

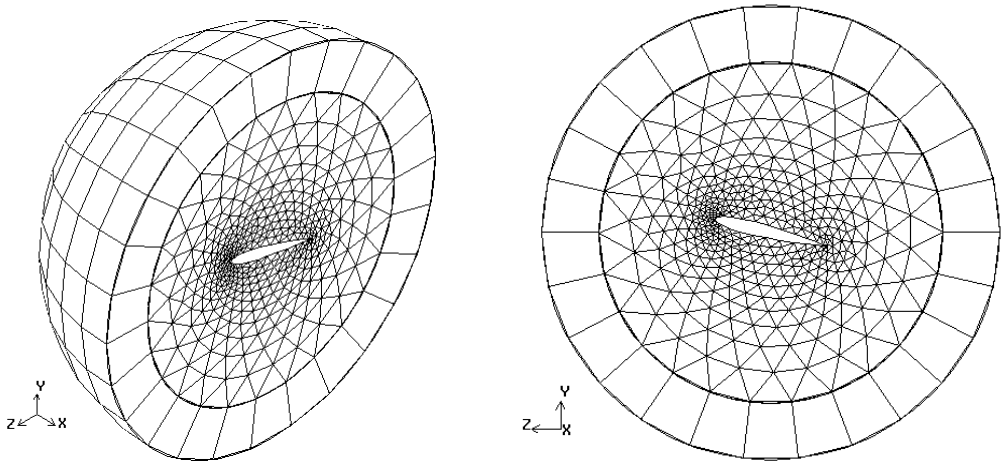

a) 3-D view **b) 2D view**

Fig. 8. Interior sphere after manipulating the nodes connection of shell elements.

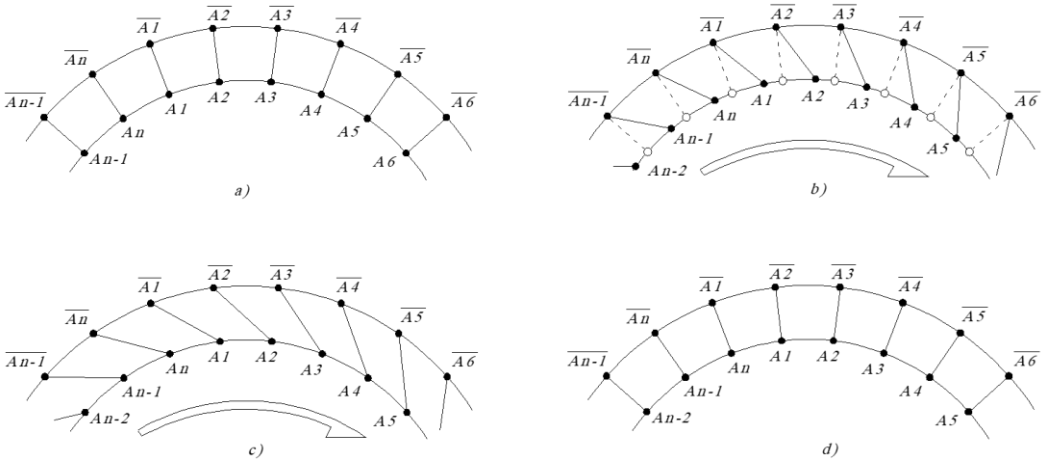

a) Before rotation
b) After rotation of the inner part
c) After rotation when each node on the inner part reaches the previous position of its neighbor node
d) After rotation and manipulating the nodes connection

Fig. 9. Connections manipulation process in the shell elements.

Table 1 Renumbering in data structure of the shell elements, colored cells are variable

Elements No.	1		2		…		n-1		n	
Nodes before manipulating the connections	$\overline{A1}$	$\overline{A2}$	$\overline{A2}$	$\overline{A3}$	…	…	$\overline{An-1}$	$\overline{An}$	$\overline{An}$	$\overline{A1}$
	A1	A2	A2	A3	…	…	An-1	An	An	A1
Nodes after 1 manipulating the connections	$\overline{A1}$	$\overline{A2}$	$\overline{A2}$	$\overline{A3}$	…	…	$\overline{An-1}$	$\overline{An}$	$\overline{An}$	$\overline{A1}$
	An	A1	A1	A2	…	…	An-2	An-1	An-1	An
Nodes after 2 manipulating the connections	$\overline{A1}$	$\overline{A2}$	$\overline{A2}$	$\overline{A3}$	…	…	$\overline{An-1}$	$\overline{An}$	$\overline{An}$	$\overline{A1}$
	An-1	An	An	A1	…	…	An-3	An-2	An-2	An-1
.	…	…	…	…	…	…	…	…	…	…
	…	…	…	…	…	…	…	…	…	…

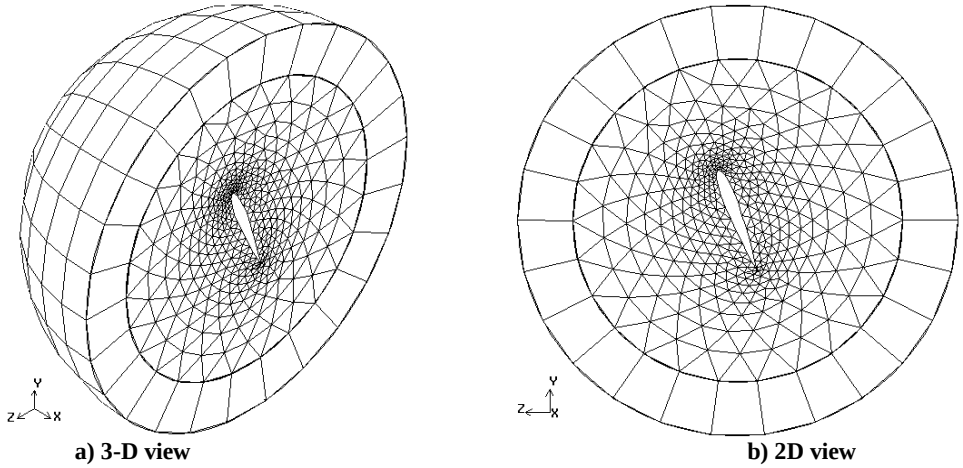

a) 3-D view **b) 2D view**

Fig. 10. Interior sphere after 70° rotation of wing and 5 phases of connections' manipulation.

Through this method, the body can rotate freely without experiencing any major deformation in grid elements. The only necessity is that the connection nodes are reformed considering the amount of rotation. The written software manipulates the connections regarding the rotation degree without the interference of user (Fig. 10). Therefore, using this method, the grid is able to adapt to any rotation or oscillation with no need to re-mesh. Also, with known deformable elements, there is no need to use an algorithm search to find deformed elements. In addition, the quality of elements is maintained even in large motions of the body and a grid with high quality is always available for the user. As for a limitation of the presented moving grid method, the incapability of modeling the simultaneous rotation of two bodies with a small distance can be mentioned.

5. SOLUTION ALGORITHM

The three dimensional unsteady compressible Euler equations in the Cartesian coordinate system can be written as

$$\frac{\partial Q}{\partial t}+\frac{\partial F}{\partial x}+\frac{\partial G}{\partial y}+\frac{\partial H}{\partial z}=0 \tag{1}$$

Where Q, the vector of conserved quantities, is given as

$$Q=\begin{bmatrix}\rho\\ \rho u\\ \rho v\\ \rho w\\ \rho E\end{bmatrix} \tag{2}$$

And the convective fluxes F, G and H in the corresponding x, y and z coordinate directions are defined as

$$F=\begin{bmatrix}\rho u_r\\ \rho u_r u+P\\ \rho u_r v\\ \rho u_r w\\ (\rho E+P)u_r+x_t P\end{bmatrix}$$

$$G=\begin{bmatrix}\rho v_r\\ \rho v_r u\\ \rho v_r v+P\\ \rho v_r w\\ (\rho E+P)v_r+y_t P\end{bmatrix} \tag{3}$$

$$H=\begin{bmatrix}\rho w_r\\ \rho w_r u\\ \rho w_r v+P\\ \rho w_r w+P\\ (\rho E+P)w_r+z_t P\end{bmatrix}$$

Where $\rho, P, u, v, w, x_t, y_t, z_t, u_r, v_r, w_r$and E denote density, pressure, Cartesian velocity components, Cartesian velocity components of control-volume boundary, relative velocities and total energy

respectively.

The relative velocities are defined as

$$u_r = u - x_t, \qquad v_r = v - y_t, \qquad w_r = w - z_t$$

The Eq. (1) are augmented by the equation of state, which for a perfect gas is given by

$$P = (\gamma - 1)\left[\rho E - \rho\frac{u^2 + v^2 + w^2}{2}\right] \tag{4}$$

Where γ is the ratio of specific heat.

For a control volume with volume v and surface s, Eq.(1) can be rewritten in integral form as

$$\frac{\partial}{\partial t}\iiint_v Q dV + \oiint_S \left(\frac{\partial F}{\partial x} + \frac{\partial G}{\partial y} + \frac{\partial H}{\partial z}\right) dS = 0. \tag{5}$$

Appling Eq. (5) to each cell in the domain independently, the spatial and time dependent terms are decoupled and a set of ODE`s is obtained in the following form

$$\frac{d}{dt}(Q_i V_i) + R_i(Q) = 0 \tag{6}$$

That first term of above equation indicant change in control-volume depend of time and $R_i(Q)$ is the convective fluxes of cell faces. Where V_i is the cell volume, considering the fact that the form of the elements outside the spherical shell is constant, these elements will have no volume change in relation to time. Of course, no volume changes occur in the shell elements in rotational motions due to the existence of symmetry. Therefore, we may conclude that the volume of all elements is constant in relation to time and Eq. (6) can be rewritten accordingly:

$$V_i \frac{d}{dt}(Q_i) + R_i(Q) = 0 \tag{7}$$

The properties over each cell faces are evaluated using an averaging method. In this method added numerical dissipative term to Eq. (7) with using Jameson method (Jameson, Schmidt, and Turkel 1981; Jameson and Mavriplis 1986).

$$V_i \frac{d}{dt}(Q_i) + R_i(Q) - D_i(Q) = 0 \tag{8}$$

The numerical dissipative term in three dimensional is defined as

$$D_i(Q) = \sum_{K=1}^{N} d_{ik} \tag{9}$$

Where d_{ik} of numerical dissipative terms at the boundary face cells i and k, is defined as

$$d_{ik} = \left(\frac{V_i}{\Delta t} + \frac{V_k}{\Delta t}\right)\left[\frac{\epsilon_{ik}^2}{2}(Q_i - Q_k) + \frac{\epsilon_{ik}^4}{2}(\nabla^2 Q_i - \nabla^2 Q_k)\right] \tag{10}$$

where

$$\nabla^2 Q_i = \sum_{K=1}^{n} (Q_k - Q_i),$$

$$\epsilon_{ik}^2 = k_2 \max(v_{ik}),$$

$$\epsilon_{ik}^4 = \max(0, k_4 - \epsilon_{ik}^2),$$

$$v_{ik} = \left|\frac{P_i - P_k}{P_i + P_k}\right|$$

And the constant values k_2 and k_4 are

$$k_2 = 0.9$$

$$k_4 = 0.02$$

For time integration of equations used an implicit dual time method (Jameson 1991; Gaitonde 1994; Jahangirian and Hadidoolabi 2004), in real time a second order accurate backward difference formula (BDF) is used as follows

$$V_i\left[\frac{3}{2\Delta t}(Q_i{}^{n+1}) - \frac{2}{\Delta t}(Q_i{}^{n}) + \frac{1}{2\Delta t}(Q_i{}^{n-1})\right] + R_i(Q^{n+1}) - D_i(Q^{n+1}) = 0 \tag{11}$$

With rewriting above equation in each time step

$$V_i \frac{\partial Q_i{}^{n+1}}{\partial \tau} + R_i^*(Q^{n+1}) = 0 \tag{12}$$

Where τ is pseudo-time and $R_i^*(Q^{n+1})$ is the unsteady residual, that is given by

$$R_i^*(Q^{n+1}) = V_i\left[\frac{3}{2\Delta t}(Q_i{}^{n+1}) - \frac{2}{\Delta t}(Q_i{}^{n}) + \frac{1}{2\Delta t}(Q_i{}^{n-1})\right] + R_i(Q^{n+1}) - D_i(Q^{n+1}) \tag{13}$$

For solving Eq. (12) an explicit Runge-Kutta multistage method is used, the four-stage Runge-Kutta method is given by

$$Q^{(0)} = (Q_i^{n+1})^m$$

$$Q^{(1)} = Q^{(0)} - \alpha_1 \frac{\Delta\tau}{V_i} R_i^*(Q^{(0)})$$

$$Q^{(2)} = Q^{(0)} - \alpha_2 \frac{\Delta\tau}{V_i} R_i^*(Q^{(1)})$$

$$Q^{(3)} = Q^{(0)} - \alpha_3 \frac{\Delta\tau}{V_i} R_i^*(Q^{(2)})$$

$$Q^{(4)} = Q^{(0)} - \alpha_4 \frac{\Delta\tau}{V_i} R_i^*(Q^{(3)})$$

$$(Q_i^{n+1})^{m+1} = Q^{(4)}$$

Where

$$R_i^*(Q^l) = V_i\left[\frac{3}{2\Delta t}(Q_i{}^{l}) - \frac{2}{\Delta t}(Q_i{}^{n}) + \frac{1}{2\Delta t}(Q_i{}^{n-1})\right] + R_i(Q^l) - D_i(Q^0).$$

And typical values of the constant $\alpha_1, \alpha_2, \alpha_3$ and α_4 are

$$\alpha_1 = 0.333$$

$$\alpha_2 = 0.2667$$

$$\alpha_3 = 0.555$$

$$\alpha_4 = 1.0$$

to accelerate convergence, local pseudo-time

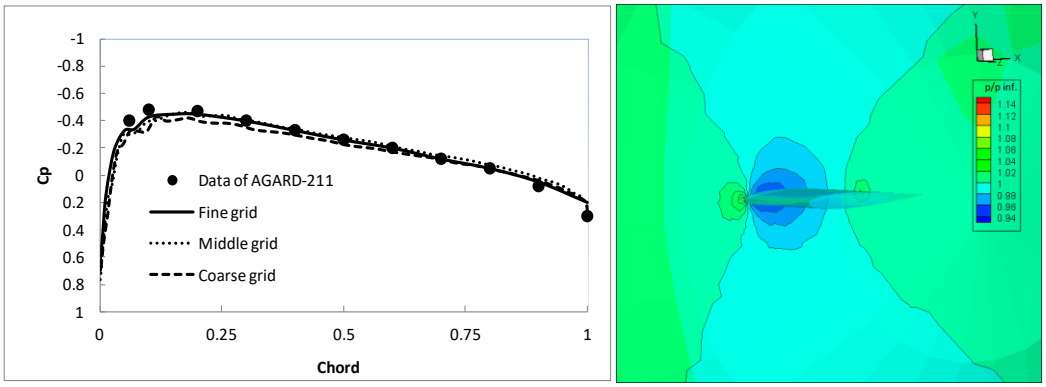

a) Comparison of pressure distribution **b) pressure contour at the middle of span**

Fig. 11. The NACA0012 airfoil in subsonic flow with $M_\infty = 0.5, \propto = 0^\circ$.

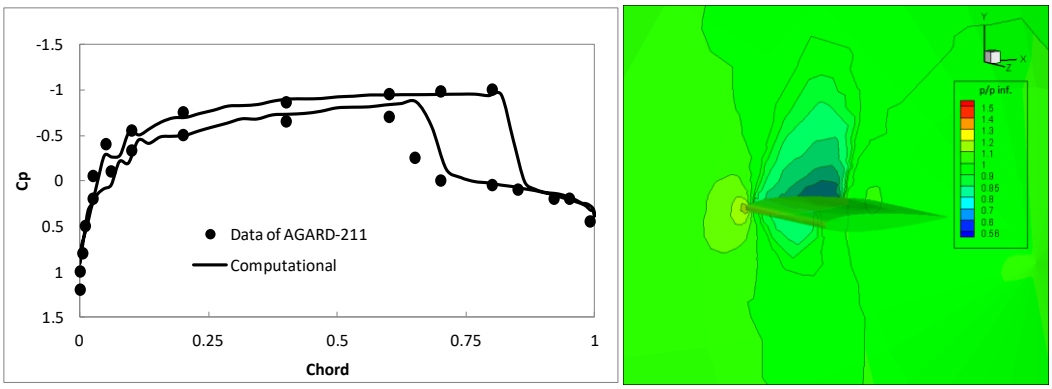

a) Comparison of pressure distribution **b) pressure contour at the middle of span**

Fig. 12. The NACA0012 airfoil in transonic flow with $M_\infty = 0.85, \propto = 1^\circ$.

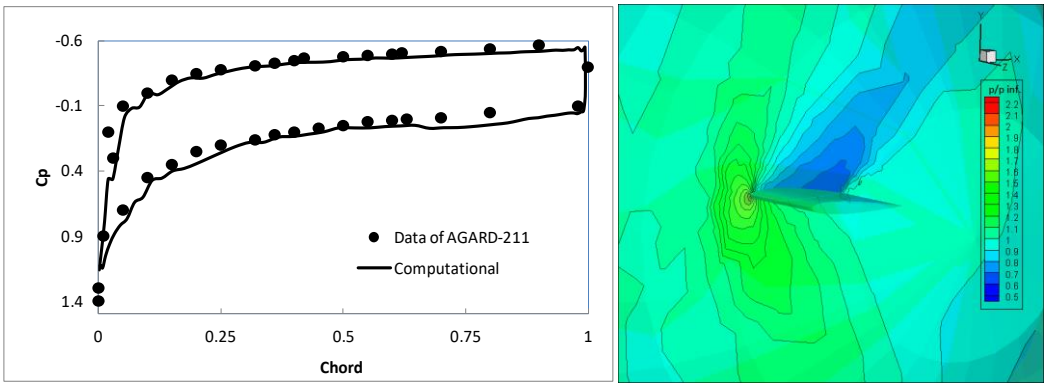

a) Pressure distribution **b) pressure contour at the middle of span**

Fig. 13. The NACA0012 airfoil in supersonic flow with $M_\infty = 1.2, \propto = 7^\circ$.

stepping, enthalpy damping and residual averaging are used (Jameson, Schmidt, and Turkel 1981).

In the far field, non-reflecting boundary conditions are used based on the characteristic analysis. At the solid wall boundary, the normal velocity is set equal to zero, since no mass or other convective fluxes can penetrate the solid body. The pressure value at the solid wall can be obtained by extrapolating from the values of adjacent cells.

6. NUMERICAL RESULT

To validate and demonstrate the correct performance of solver and grid, several test cases have been solved. These include a rectangular wing with NACA0012 airfoil in subsonic flow with $M_\infty = 0.5, \propto = 0^\circ$, transonic flow with $M_\infty = 0.85, \propto = 1^\circ$ and supersonic flow with $M_\infty = 1.2, \propto = 7^\circ$. The chord has a length of 1, the wing span is 4. The radius of outer boundary is 7 and thickness of spherical shell is 0.7.

The C_P distributions obtained on the wing surface at the middle of span and pressure contours are shown in Figs 11-13. The calculated results agree very well with the results of AGARD-211.

Table 2 Grid specifications

Grid type	Number of nodes	number of elements	Number of nodes on each airfoil	Number of nodes on the wing	Number of elements on the wing
Coarse	13988	74995	100	2395	4786
Middle	37451	198465	150	8330	16656
fine	72675	358992	200	14113	28222

It should be mentioned that the above results are obtained after the grid study for each case. For the subsonic case, three different grids are used. As is seen, although the results change from coarse grid to middle grid, the results of middle grid and fine grid are the same. Therefore, the middle grid is chosen. This is the case for other solutions as well. The grid specifications for all of these cases are given in Table2.

The convergence history for employed grid is shown in Fig. 14. The error is defined as the density difference calculated between two successive time steps that 10^{-8} for real time and 10^{-3} for pseudo time is considered. Due to the small number of the real time steps for convergence (smaller 4) and the number of the pseudo time steps at each real time step (smaller 3) except for the first step, therefore iterations in the first step of real time is used for convergence history. Number of iterations is 508 and total time necessary for convergence of solver in subsonic flow is 240 seconds.

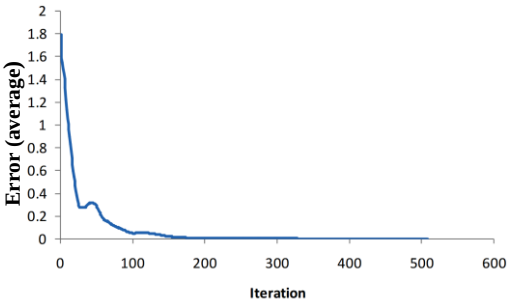

Fig. 14. Convergence history for the solution of flow around airfoil.

Now it is time to demonstrate that without interpolation and only with element renumbering, the accuracy of solution would not be lost in a rotational motion. The oscillatory wings with NACA0012 airfoil studied, which undergoes harmonic pitching motion about the quarter chord with the following time dependent angle of attack $\propto = \alpha_m + \alpha_0 \sin\omega t$, where α_m is the meanangle of attack, α_0 is the oscillation amplitude and ω is the angular frequency of the motion which is related to reduce frequency K by $K = \omega c/2V_\infty$, where V_∞ is the free stream velocity and c is the chord length of the airfoil.

The flow conditions over the wing are $M_\infty = 0.6, \alpha_m = 2.89°, \alpha_0 = 2.41°$ and $K = 0.0808$, that is similar to AGARD CT1. The comparison of normal force coefficient with experimental data is shown in Fig. 15. As is seen the computed result agree very well with the experimental result.

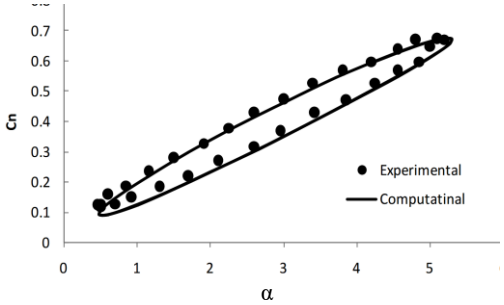

Fig. 15. Normal force coefficient for CT1 test case.

Another flow conditions are $M_\infty = 0.755, \alpha_m = 0.016^\circ, \alpha_0 = 2.51^\circ$ and $K = 0.0814$, that is similar to AGARD CT5. The comparison of normal force and pitching moment coefficient with experimental data is shown in Figs 16 and 17. It is obvious that the agreement is good, indicating that the implementation of the present algorithm is successful.

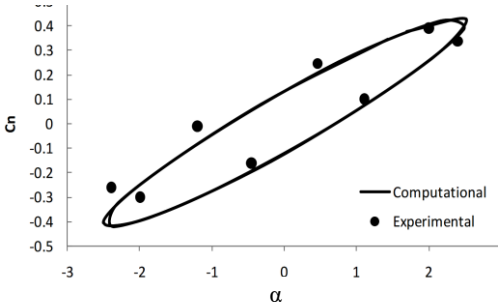

Fig. 16. Normal force coefficient for CT5 test case.

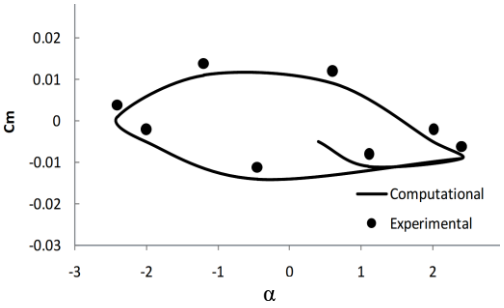

Fig. 17. Pitching moment coefficient for CT5 test case.

7. CONCLUSION

We could simulate rotational motion and oscillation of the body by dividing a solution domain around the body into three spherical regions. Each region is used for modeling the rotation around one of the three axes, and the general rotations of the body are simulated in general. Using the orbital and meridian form for surface elements of each sphere and manipulating the grid connections through a defined algorithm, the reduction of the grid quality id prevented and we can simulate rotational motion even up to 360 degrees without any interpolation. The computational results show good consistency between this method and the previous experimental data.

REFERENCES

AGARD Advisor report No. 211, Test Cases for Inviscid Flow Field Methods.

AGARD-R-702, (1982), Compendium of unsteady aerodynamic measurements.

Batina, J. T. (1989). Unsteady Euler airfoil solutions using unstructured dynamic mesh, *27th Aerospace Meeting, Reno, Nevada* (0115).

Batina, J. T. (1991). Unsteady Euler algorithm with unstructured dynamic mesh for complex airfoil aerodynamic analysis, *AIAA Journal* 29(3).

Cai, j., H. M. Tsai and F. Liu (2005). A parallel viscous flow solver on multi-block overset grids, *computer & fluid* 39(6), 1021-1029.

Degand, C. and C. Farhat (2002). A three-dimensional torsional spring analogy method for unstructured dynamic meshes, *Computer and Structure* 80, 305-316.

Gaitonde, A. L. (1994). A dual-time method for the solution of the unsteady Euler equations, Aeronautical journal 283-291.

Gaitonde, A. L. and S. P. Fiddes (1995). A three-dimensional moving mesh method for the calculation of unsteady transonic flows, *Aeronautical Journal* (2011).

Goswami, A. and I. H. Parpia (1991). Grid restructuring for moving boundaries, *AIAA Journal* (1589).

Hase, J. E., D. A. Anderson and I. H. Parpia (1991). A Delaunay triangulation method and Euler solver for bodies in relative motion, *AIAA Journal* (1590).

Jahangirian, A. and M. Hadidoolabi (2004). An implicit solution of the unsteady Navier-Stokes equations on unstructured moving grids, 24th International Congress of the Aeronautical Science.

Jameson, A. (1991). Time-dependent calculations using multi-grid with applications to unsteady flows past airfoils and wings, AIAA 91-1596.

Jameson, A. and D. Mavriplis (1986). Finite volume solution of the two dimensional Euler equation on a regular triangular mesh, AIAA 24(4).

Jameson, A. W. Schmidt and E. Turkel (1981). Numerical solution of the Euler equations by finite volume methods using Runge-Kutta time stepping schemes, AIAA 81-1259.

Kamkar, S. J., A. M. Wissink, V. Sankaran and A. Jameson (2012). Combined Feature-Driven Richardson-Based Adaptive Mesh Refinement for Unsteady Vortical Flows 50(12), 2834-2847.

Kannan, R. and Z. J. Wang (2006). A Parallel Overset Adaptive Cartesian/Prism Grid Method for moving boundary flows', *Proceedings of the Fourth International Conference on Computational Fluid Dynamics, ICCFD*, Ghent, Belgium 323-328.

Kannan, R. and Z. J. Wang (2007). Overset Adaptive Cartesian/Prism Grid Method for Stationary and Moving-Boundary Flow Problems, *AIAA* 45(7), 1774-1779.

Karimian, S. M. H. and M. Ardakani (2011). Immersed Boundary Method for the Solution of 2D Inviscid Compressible Flow Using Finite Volume Approach on Moving Cartesian Grid, *Journal of applied fluid mechanics* 4(3), 27-36.

Liu, J., and H. Akay (2010). Flow around moving bodies using a dynamic unstructured overset-grid method, *international journal of computational fluid dynamics* 4(5), 23-36.

Mirsajedi, S. M. and S. M. H. Karimian (2006a). Evaluation of a two-dimensional Moving-Mesh Method for Rigid Body Motions, *Aeronautical Journal* 429-438.

Mirsajedi, S. M. and S. M. H. Karimian (2006). Unsteady Flow Calculations with a New Moving-Mesh Algorithm, *AIAA* (1153).

Mirsajedi, S. M., S. M. H. Karimian and M. Mani (2006). A Multi Zone Moving Mesh Algorithm for Simulation of Flow Around a Rigid Body With Arbitrary Motion, *ASME Journal of Fluids Engineering* 128, 297-304.

Ou, K., P. Castonguay and A. Jameson (2011). Computational Sports Aerodynamics of a Moving Sphere: Simulation a Ping Pong Ball in Free Flight, *Aerodynamics Conference*, Honolulu, HI.

Ou, K. and A. Jameson (2010). On the Temporal and Spatial Accuracy of Spectral Difference Method on Moving Deformable Grids and the Effect of Geometry Conservation Law, *AIAAJournal* (5032), *40th AIAA Fluid Dynamics Conference and Exhibit*, Chicago, Illinois.

Ou, K. and A. Jameson (2011). Dynamic Mesh Deformation for Adaptive Grid Resolution Enhancement with Staggered Spectral Difference and Finite Volume Mesh, *AIAAJournal* (196), 49th AIAA Aerospace Sciences Meeting, Orlando, Florida.

Pirzadeh, S. Z. (1999). An Adaptive Unstructured Grid Method by Grid Subdivision, Local Remeshing and Grid Movement, *14th AIAA Journal* (3255).

Srinivasa Rao, V. and L. Babu (2013). Finite Element Analysis of Radiation and Mass Transfer Flow Past Semi- Infinite Moving Vertical Plate with Viscous Dissipation, *Journal of applied fluid mechanics* 6(3), 321-329.

Togashi, F., Y. Ito, K. Nakahashi and S. Obayashi (2006). Extensions of Overset Unstructured Grids to Multiple Bodies in Contact *Journal Aircraft* 43(1), 52-57.

Younis, Y., A. Bibi, A. U. Haque and S. Khushnood (2009). Vortical Flow Topology on Windward and Leeward side of Delta Wing at Supersonic Speed, *Journal of applied fluid mechanics* 2(2), 13-21.

Zeng, D. and C. R. Ethier (2005). A semi-torsional analogy model for updating unstructured meshes in 3-D moving domains, *Finite Elements in Analysis and Design* 41, 1118-1139.

Zhang, L. P. and Z. J. Wang (2004). A block LU-SGS implicit dual time-stepping algorithm for hybrid dynamic meshes, *computer & fluid* 33, 891-916.